Energy Band Structure of Silicon Under Uniaxial Stress in the (110) Plane Along an Arbitrary Direction

Jian-Li Ma,[1,*] He-Ming Zhang,[1] Jian-Jun Song,[1] Qun Wei,[2]
Xiao-Yan Wang,[1] Guan-Yu Wang,[1] and Xiao-Bo Xu[1]

[1]*Key Laboratory of Ministry of Education for Wide Band-Gap Semiconductor Materials and Devices, Xidian University, Xi'an, Shannxi 710071, P.R. China*

[2]*School of Science, Xidian University, Xi'an, Shannxi 710071, P.R. China*

(Received August 31, 2010)

The strain tensors arising from a uniaxial stress along an arbitrary direction in the (110) plane are calculated. With these uniaxial strain tensors, the energy band structure of the silicon material under arbitrary uniaxial stress in the (110) plane is modeled using deformation potential theory and six-band $k \cdot p$ perturbation theory. The relation between the energy band structure and the stress (type, direction, and magnitude of stress) is obtained. The effects of the uniaxial stress on the band structure (such as the conduction band (CB) and valence band (VB) edge energy levels, the CB and VB splitting energies, and the bandgap) are clarified. The calculated band structure suggests that the uniaxial stress along the <001> direction for electrons, and along the <110> direction for holes, can induce a large carrier mobility change. These band structure results can be used as a guide for the design and the selection of the optimum stress/channel configuration of uniaxial strained silicon devices.

PACS numbers: 71.70.Fk, 71.18.+y, 71.15.-m

I. INTRODUCTION

Due to high carrier mobility, energy band structure adjustment, and process compatibility with current silicon process technology, strained silicon technology is becoming the preferred method for enhancing the mobility of the carriers for high-speed metal-oxide-semiconductor field effect transistors (MOSFET). [1]. The ways of introducing strain into the channel include substrate-induced biaxial strain and process-induced uniaxial strain [2, 3]. Uniaxial strain has many advantages over biaxial strain, such as a large hole mobility enhancement at low stress, a high vertical electric field, and a small threshold voltage shift, which has made uniaxial strain the current mainstream technology [4].

The optimal stress configuration (type, direction, and magnitude of stress) can significantly change the energy band structure, inducing a shift and splitting of the conduction/valence band edge energy level, which were the cause of suppressing the scattering

*Electronic address: jianlima2005@126.com

 © 2011 THE PHYSICAL SOCIETY OF THE REPUBLIC OF CHINA

and lowering of the effective mass, thus leading to the electron/hole mobility having a large enhancement. Previous studies mainly concentrated on the effect of biaxial strain on the electrical-characteristics of the silicon material, inversion layer, and MOSFET [5–7]. Recently, the effect of biaxial strain on the energy band structure of the silicon material has been intensively investigated [8–10]. However, few studies have focused on the impact of uniaxial stress on the energy band structure of silicon material.

In this paper, a uniaxial stress in the (110) plane along an arbitrary direction is applied to the silicon crystal, this covers the cases for the stress along the most principal three crystallographic directions, such as the <001>, <111>, and <110> directions. By changing the stress type (tensile, compressive), direction, and magnitude in the (110) plane, the energy band structure of silicon, such as the shift and splitting of the band edge energy level and the bandgap change, with stress is systemically studied. Based on these band structure results, we demonstrated that uniaxial stress along the <001> direction for an electron and along the <110> direction for a hole is most favorable for enhancing the electron/hole mobility from the viewpoint of the energy band structure.

II. CALCULATED MODELS

II-1. Uniaxial strain tensor for the (110) plane arbitrary direction stress

To calculate the energy band structure of silicon under the application of uniaxial stress, the strain tensor is necessary. The strain tensor for the (110) plane with arbitrary direction uniaxial stress can be obtained as follows:

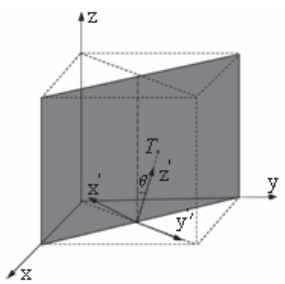

FIG. 1: The schematic figure for the uniaxial strain tensor calculation, where the stress is in the (110) plane along an arbitrary direction.

Considering a uniaxial stress of magnitude T (positive for tensile stress, and negative for compressive stress) along a direction in the (110) plane, the analysis begins by adopting a coordinate system (x', y', z'), where the z' axis is parallel to the direction of the stress T, and the y' axis is perpendicular to the (110) plane (see Fig. 1). In the coordinate system

(x', y', z'), the stress tensor has the form

$$T' = \begin{bmatrix} 0 & 0 & 0 \\ 0 & 0 & 0 \\ 0 & 0 & T \end{bmatrix}. \tag{1}$$

To transform the stress tensor from the coordinate system(x', y', z') to the crystal coordinate system (x, y, z), the transformation U is used, where

$$U = \begin{bmatrix} \frac{1}{\sqrt{2}}\cos\theta & \frac{1}{\sqrt{2}}\cos\theta & \frac{1}{\sqrt{2}}\sin\theta \\ -\frac{1}{\sqrt{2}}\sin\theta & \frac{1}{\sqrt{2}}\cos\theta & \frac{1}{\sqrt{2}}\sin\theta \\ 0 & -\sin\theta & \cos\theta \end{bmatrix}. \tag{2}$$

Here the angle θ is the polar angle between z' and z. Using the relationship between the coordinate systems for tensors, the stress tensor in the crystal coordinate system (x, y, z) can be calculated from

$$T_{ik} = U_{ij}U_{kl}T'_{jl}. \tag{3}$$

Here, the i, j, and k stand for x, y, and z, respectively.

The strain tensor can be obtained from the stress tensor by the inversion of Hooke's law

$$\varepsilon_{ij} = s_{ijkl}T_{kl}, \tag{4}$$

where s_{ijkl} represents the cubic elastic compliance tensor of silicon, and ε_{ij} denotes the strain tensor. Using the above relation, the strain tensor for a uniaxial stress of magnitude T along a direction in the (110) plane can be obtained as

$$\begin{aligned} \varepsilon_{xx} &= \varepsilon_{yy} = T\left[\frac{1}{2}s_{11}\sin^2\theta + \frac{1}{2}s_{12}\sin^2\theta + \cos^2\theta)\right], \\ \varepsilon_{zz} &= T(s_{11}\cos^2\theta + s_{12}\sin^2\theta), \\ \varepsilon_{xy} &= \frac{1}{2}Ts_{44}\sin^2\theta, \\ \varepsilon_{xz} &= \varepsilon_{yz} = \frac{1}{2\sqrt{2}}Ts_{44}\sin\theta\cos\theta. \end{aligned} \tag{5}$$

Values for s_{11}, s_{12}, and s_{44} are given in Table I.

II-2. Band structure calculation

The conduction band of unstrained Silicon has six equivalent energy valleys along the Δ direction (<100> direction) of the Brillouin zone, and the constant energy surfaces are ellipsoids of revolution whose major axes is along the Δ direction. The energy for the conduction band valley under strain is

$$E_c^i = E_c^0 + \delta E_c^i, \tag{6}$$

where i stands for the valley, E_c^0 represents the energy of the conduction band valley minima without strain, and δE_c^i denotes the energy shift of the valley i under strain, which can be calculated for the Δ valleys and Γ valley according to the deformation potential theory as

$$\delta E_c^{\Delta} = \Xi_d^{\Delta}\mathrm{Tr}(\hat{s}) + \Xi_u^{\Delta}\varepsilon_{ii} \tag{7}$$

and

$$\delta E_c^{\Gamma} = a_c^{\Gamma}\mathrm{Tr}(\hat{s}), \tag{8}$$

respectively. Here $\mathrm{Tr}(\hat{s}) = \varepsilon_{xx} + \varepsilon_{yy} + \varepsilon_{zz}$, while Ξ_d^{Δ}, Ξ_u^{Δ}, and a_c^{Γ} are conduction band deformation potential constants, which are given in Table I.

As for the valence band, the valence band energy maximum of silicon located at the center of the Brillouin zone (Γ point), is a six-fold degenerate multiplet state in the absence of strain and the spin-orbit effect. Taking into account the spin-orbit coupling effect, the valence band consists of a four-fold degenerate Γ_8 band and a two-fold degenerate Γ_7 band (with respect to the spin-orbit coupling band), and the energy difference between the Γ_8 and Γ_7 band is $\Delta = 0.044$ eV.

The spin-orbit coupling Hamiltonian H_{so} can be expressed as

$$H_{\mathrm{so}} = -\frac{\Delta}{3}\begin{bmatrix} 0 & i & 0 & 0 & 0 & -1 \\ -i & 0 & 0 & 0 & 0 & i \\ 0 & 0 & 0 & 1 & -i & 0 \\ 0 & 0 & 1 & 0 & -i & 0 \\ 0 & 0 & i & i & 0 & 0 \\ -1 & -i & 0 & 0 & 0 & 0 \end{bmatrix}. \tag{9}$$

Introduce uniaxial strain into the silicon; the strain can be regarded as a perturbation term to the total of valence band Hamiltonian. The valence band strain perturbation Hamiltonian H_ε has the form

$$H_\varepsilon = \begin{bmatrix} H'' & 0_{3\times3} \\ 0_{3\times3} & H'' \end{bmatrix} \begin{matrix} \uparrow \\ \downarrow \end{matrix}, \tag{10}$$

and

$$H'' = \begin{bmatrix} l\varepsilon_{xx} + m(\varepsilon_{yy} + \varepsilon_{zz}) & n\varepsilon_{xy} & n\varepsilon_{zx} \\ n\varepsilon_{xy} & l\varepsilon_{yy} + m(\varepsilon_{xx} + \varepsilon_{zz}) & n\varepsilon_{yz} \\ n\varepsilon_{zx} & n\varepsilon_{yz} & l\varepsilon_{zz} + m(\varepsilon_{xx} + \varepsilon_{yy}) \end{bmatrix}. \tag{11}$$

Here, the l, m, and n are valence band deformation potential constants, and the values are given in Table I.

By diagonalizing the matrix of $H_{\mathrm{so}} + H_\varepsilon$, one can obtained the eigenvalues of this matrix, that is the valence band energy at the Γ point, which takes into account the effect of spin-orbit coupling and strain. Due to space considerations, the detailed derivation procedure of the eigenvalues for the $H_{\mathrm{so}} + H_\varepsilon$ matrix cannot be given here, but it can be found in Refs. [11] and [12].

The energy for the valence band maxima under strain can be calculated as

$$E_v = E_v^0 + \delta E. \tag{12}$$

Here, E_v^0 represents the unstrained valence band maximum energy. δE denotes the valence band energy at the Γ point due to the effects of spin-orbit coupling and strain.

TABLE I. Parameters for the band structure calculation of silicon.

s_{11}, s_{12}, s_{44} (cm^2/dyn)	$a_c^\Gamma, \Xi_d^\Delta, \Xi_u^\Delta$ (eV)	l, m, n (eV)	E_c^0, E_v^0 (eV)	Δ (eV)
7.69×10^{-13}, -2.44×10^{-13}, 1.25×10^{-12}	−15.3, 1.75, 9.16	−0.15, 6.84, −5.89	1.119, 0	0.044

III. CALCULATED RESULTS AND DISCUSSION

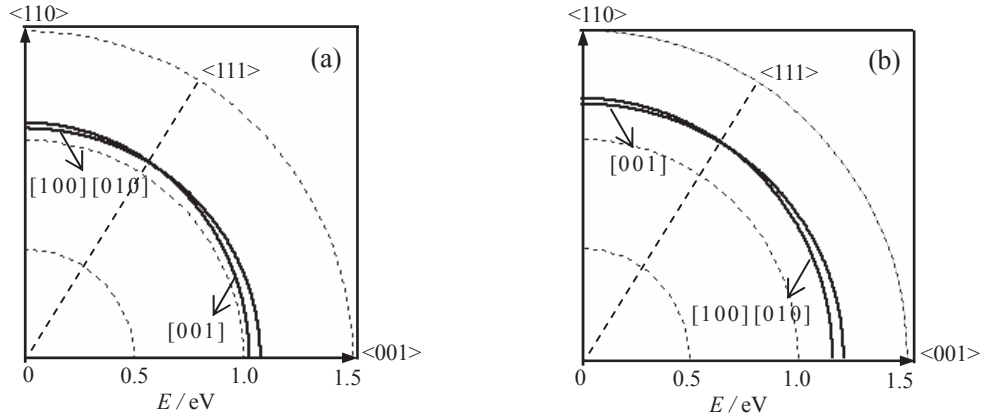

FIG. 2: The conduction band edge energy levels for the Δ valleys for various stress directions under the magnitude of 1 GPa uniaxial compressive stress (a) and 1 GPa uniaxial tensile stress (b).

FIG. 2 shows the calculated energy levels of the Δ valleys for different directions of uniaxial stress in the (110) plane. Note that the energy levels of the Δ valleys are six-fold degenerate in the absence of stress due to the face-centered cubic lattice symmetry of silicon. When the uniaxial stressed is applied, the energy levels of the Δ valleys are shifted and split, and the degeneracy of the energy levels are partly reduced or conserved.

Under 1GPa uniaxial compressive stress, the energy levels of the Δ valleys move down with respect to the unstressed case. When the stress is taken along the <001> direction, the original six-fold degenerate energy levels split into two pairs of energy levels, one two-fold degenerate along the [001] orientation, the other four-fold degenerate along the [100]

and [010] orientation, and the two-fold degenerate energy level has a lower energy. With the stress along the <111> direction, the energy levels remain six-fold degenerate. For the <110> direction stress, the energy levels splitting is similar to the case in which the stress is along the <001> direction, but in this case, the four-fold degenerate energy levels along the [100] and [010] orientations have lower energy than the energy level along the [001] orientation, as shown in Fig. 2(a). Under 1 GPa uniaxial tensile stress, the splitting of the energy levels of the Δ valleys is similar to that of the uniaxial compressive stress case, but the band edge energy level shifts are opposite to those of the uniaxial compressive stress case (see Fig. 2(b)). Note that the calculated results of our energy level shift trend and splitting case for the Δ valleys under uniaxial <001> and <110> stress are consistent with the recently published results based on the empirical pseudopotential method (EPM) and the first principle simulation [13, 14]. The shift and splitting of the energy levels of the Δ valleys can be explained from the fact that when the uniaxial stress is applied to the silicon crystal, which breaks the silicon crystal original cubic symmetry, it reduces the symmetry of the silicon crystal, thus causing a shift and splitting of the energy levels.

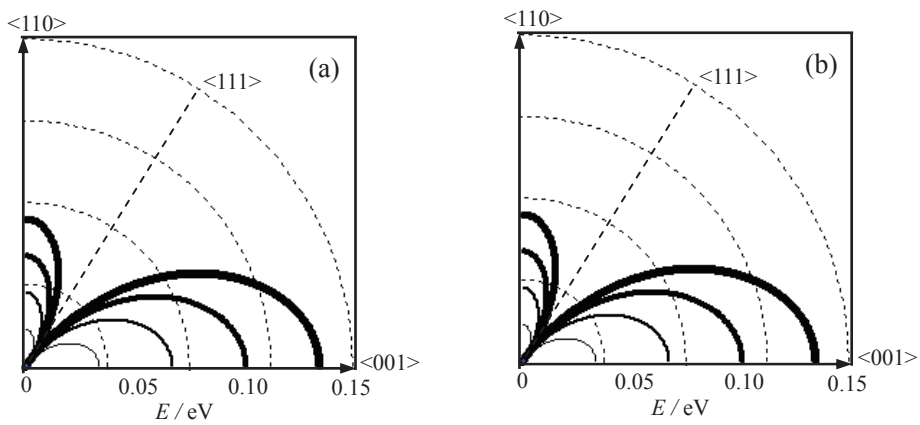

FIG. 3: The splitting energy between the 2- and 4-fold degenerate energy levels of the Δ valleys for various stress directions under magnitude 0, 0.5, 1.0, 1.5, 2.0 GPa uniaxial compressive stress (a), and 0, 0.5, 1.0, 1.5, 2.0 GPa uniaxial tensile stress (b). The thicker line indicates that the magnitude of the stress is larger.

The splitting energy (ΔE_c) of the Δ valleys between the 2- and 4-fold degenerate energy levels under different uniaxial stress are shown schematically in Fig. 3(a) and (b). When uniaxial compressive stress is applied (see Fig. 3(a)), it is observed that ΔE_c is proportional to the stress magnitude in the same stress direction. For a given stress, ΔE_c first undergoes a decrease when the stress direction changes from the <001> to the <111> direction, then it starts to increase until the stress direction is along the <110> direction, and ΔE_c along the <001> direction is larger than that of the stress along other directions at the same stress magnitude. It is suggested that uniaxial stress along the <001> direction can induce a larger electron mobility change compared with other stress directions. Due to the conduction band edge not splitting when compressive stress is applied along the <111>

direction, ΔE_c is zero in the <111> direction. The change ΔE_c under uniaxial tensile stress shows exactly the same trend of change with stress in comparison to the uniaxial compressive stress case, as shown in Fig. 3(b).

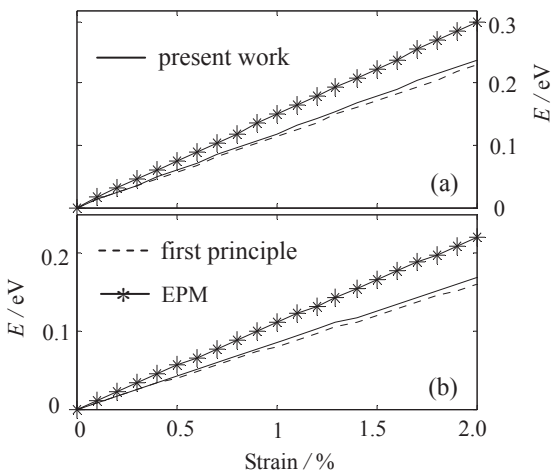

FIG. 4: Comparison of the calculated energy level splitting of the conduction band edge under (a) uniaxial <001> and (b) uniaxial <110> strain, with results from the first principle method and the empirical pseudopotential method (EPM).

For comparison, when the stress is along the <001> and <110> directions, the computed ΔE_c of the Δ valleys as a function of strain (the transformation from the stress to strain can be found in Ref. [15]) were compared with those available for the empirical pseudopotential method (EPM) and the first principle method [13, 14]. As shown in Fig. 4, it is found that our results are in good agreement with the first principle results, but a little smaller than the EPM results. Since experimental information for the energy level shift of silicon under uniaxial stress is still lacking, we only have given the results predicated by the different theories . It should be noted that the ΔE_c of bulk silicon is comparable to that of silicon nanowire. For example, at a 1% uniaxial tensile strain along the <100> direction, ΔE_c is 0.13 eV for bulk silicon, and 0.16 eV for silicon nanowire [16].

To illustrate the band gap change of bulk silicon in the uniaxial stress case, the conduction band energy level for the Γ valley under different stresses was calculated and is shown in Fig. 5. It can be seen that the energy level for the Γ valley is insensitive to the stress direction, and the energy levels for the Γ valley, are 4.3, 4.1, and 3.9 eV at 1 GPa uniaxial compressive stress, at unstressed, and at 1 GPa uniaxial tensive stress, respectively. Note that these energies for the Γ valley under stress are much larger than those of the Δ valleys, and the conduction band minimum remains located at the Δ valleys, this indicates that the bulk silicon in the uniaxial strained case is still an indirect band gap semiconductor. This is different from silicon nanowire, where there exists a band gap transition from the direct to indirect in the uniaxial strained case [16, 17].

The effects of the different directions of uniaxial stress on the valence band edge energy

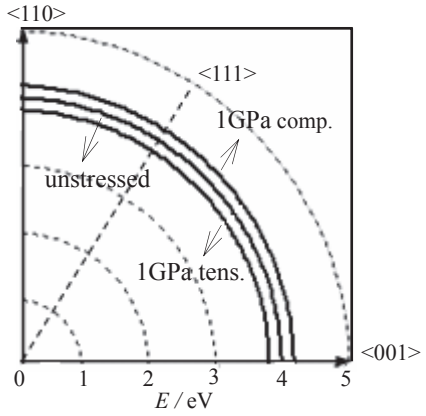

FIG. 5: The conduction band energy levels for the Γ valley under different stresses.

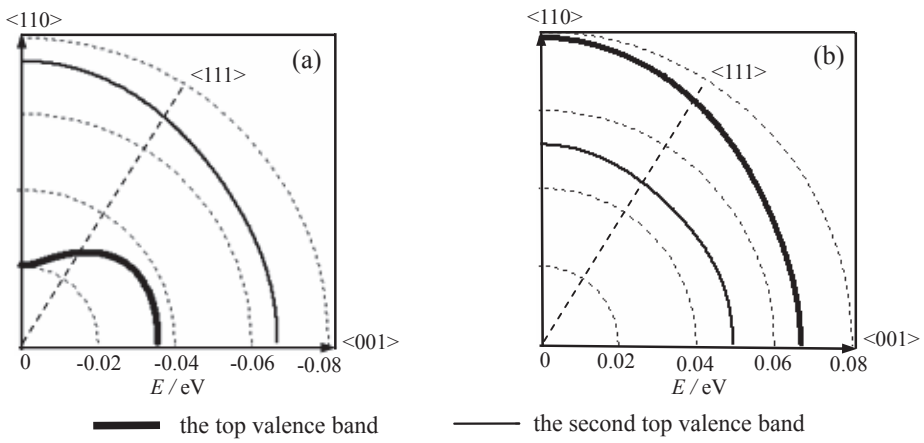

FIG. 6: The valence band edge energy for various stress directions under a magnitude of 1 GPa uniaxial compressive stress (a) and 1 GPa uniaxial tensile stress (b).

levels are presented in Fig. 6. It can be seen that the original four-fold degenerate Γ_8 band splits into a pair of two-fold degenerate $\Gamma_8^{3/2}$ bands and a pair of two-fold degenerate $\Gamma_8^{1/2}$ bands at all directions of the (110) plane under the application of 1 GPa uniaxial stress. The $\Gamma_8^{3/2}$ band and the $\Gamma_8^{1/2}$ band is namely the top and the second valence band, respectively. In silicon nanowire, the valence band edge energy levels are upshifted with respect to the unstressed case for both compressive and tensile stress [16]. However, the valence band edge energy levels of bulk silicon are downshifted with compressive stress, and are upshifted with tensile stress.

Fig. 7 gives the splitting energy (ΔE_v) between the top and the second valence band under different directions of uniaxial stress. The main feature that can be observed is that ΔE_v for the compressive stress is larger than that of the tensile stress case under the

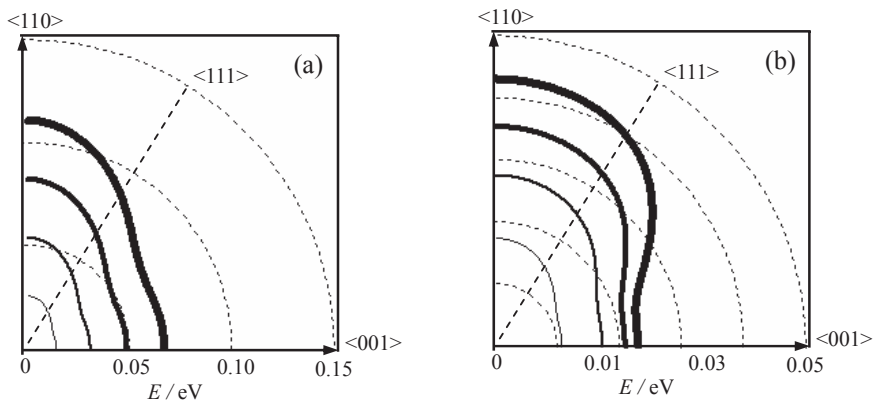

FIG. 7: The splitting energy between the top and second valence band for various stress directions under a magnitude of 0, 0.5, 1.0, 1.5, 2.0 GPa uniaxial compressive stress (a), and 0, 0.5, 1.0, 1.5, 2.0 GPa uniaxial tensile stress (b). The thicker line indicates that the magnitude of stress is larger.

same direction and magnitude of stress, which is similar to silicon nanowire in the uniaxial strained case [16]. Of all the crystallographic orientations in the (110) plane, the ΔE_v of compressive stress along the <110> direction is maximal (see Fig. 7(a)). Note that the calculated <110> direction stress induced valence band splitting energy is 0.033, 0.052, 0.072, and 0.128 eV for 0.5, 1.0, 1.5, and 2.0 GPa uniaxial compressive stress, respectively, which is consistent with the results of Thompson *et al.* [18].

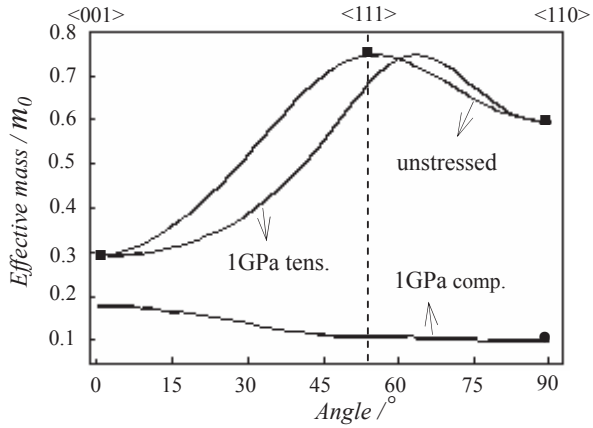

FIG. 8: The effective mass for various stress directions under unstressed, 1 GPa uniaxial tensile stress, and 1GPa uniaxial compressive stress.

In order to illustrate the effect of uniaxial stress on the valence band edge shape at the Γ point, the valence band warped at the Γ point, which can be evaluated by the effective mass, was placed under different stresses. It is supposed that the stress direction is applied along the transport direction of the charge carrier. As most of the holes incline to occupy

the top valence band, this band governed the properties of hole transport. Here, we only give the effective mass of the top valence band versus stress, as depicted in Fig. 8. The solid symbols are the calculated results using the EPM in the unstressed case along the <001>, <111>, and <110> directions from Ref. [19], and the circle symbol denotes the calculated results of 1 GPa uniaxial <110> compressive stress using $k \cdot p$ perturbation theory from Ref. [20]. For a given crystallographic direction, the effective mass of compressive stress is lower than that of the tensile stress and unstressed case. The effective mass along the <110> direction in a uniaxial compressive stress configuration is the smallest compared with other stress configurations. This is mainly because stress along the <110> direction can induce more significant shear lattice distortion than other directions, which lowers the crystal symmetry, causing severe band warping, resulting in a lower effective mass along the <110> direction. In view of suppressing the interband scattering and reducing the effective mass, the (110)/<110> configuration is most favorable to be used as the stress/channel direction for a hole, it can be expect to yield a large hole mobility change.

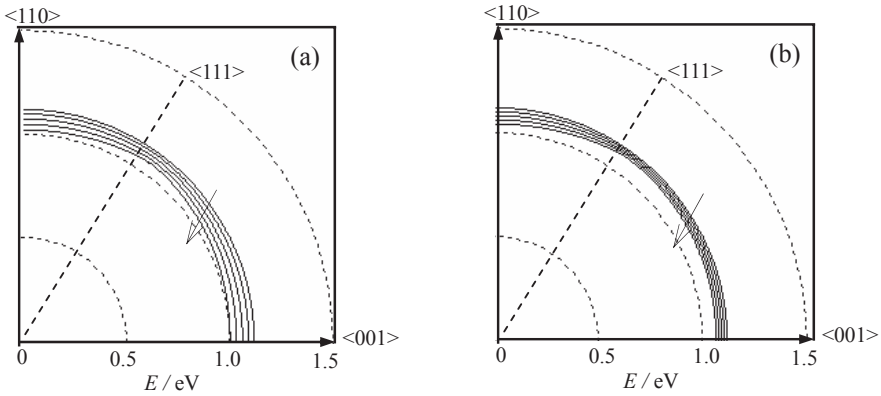

FIG. 9: The bandgap for various stress directions under the magnitude of 0, 0.5, 1.0, 1.5, 2.0 GPa uniaxial compressive stress (a) and 0, 0.5, 1.0, 1.5, 2.0 GPa uniaxial tensile stress (b). The arrow direction is the direction of stress decrease.

The bandgap is a crucial parameter for the device simulation and design of strained silicon. The effect of different directions of uniaxial stress on the bandgap are extracted from the above band structure calculation and shown in Fig. 9. It can be seen that the bandgap reduces with both compressive and tensile stress, this is similar to the silicon nanowire in the uniaxial strained case [16, 17], and the bandgap is insensitive to the stress direction whether the stress is compressive or tensile.

IV. CONCLUSIONS

The effect of a uniaxial stress along a direction in the (110) plane on the energy band structure of silicon has been examined using deformation potential theory and a six-band $k \cdot p$ perturbation theory. The results show that under the application of uniaxial stress

along a direction in the (110) plane, the compressive stress downshifts the valence and conduction band edges and the tensile stress upshifts them. The band gap of silicon is still indirect, and the bandgap reduces with the stress increasing and is almost insensitive to the stress direction. Of all crystallographic directions in the (110) plane, the splitting energy of the conduction band edge along the <001> direction is the largest for both types of stress and for a valence band edge along the <110> direction under the application of compressive stress. It is verified that compressive stress along <110> direction has a lower effective mass for a hole compared with other directions. These band structure calculated results suggested that uniaxial stress along the <001> direction for an electron, and along the <110> direction for a hole, can induced a large charge carrier mobility change.

Acknowledgements

This work is supported by the National Ministries and Commissions of China (Nos.51308040203, 6139801, and 9140C090303110C0904) and the Natural Science Basic Research Plan in Shaanxi Province of China (No.2010JQ8008).

References

[1] G. Sun *et al.*, J. Appl. Phys. **102**, 084501 (2007).
[2] C. Wee, S. Maikop, and C. Y. Yu, IEEE Circuits and Devices Magazine **21**, 21 (2005).
[3] Y. Sun *et al.*, Mater. Sci. Eng. B **135**, 179 (2006).
[4] S. E. Thompson*et al.*, IEDM Tech. Dig. **3**, 221 (2004).
[5] S. T. Chang *et al.*, Thin Solid Films **518**, 154 (2010).
[6] A. T. Phama, C. Jungemann, and B. Meinerzhagen, Solid State Electron. **52**, 1437 (2008).
[7] E. Ungersboeck *et al.*, IEEE Trans. Electron Devices **54**, 2183 (2007).
[8] D. Yu, Y. Zhang, and F. Liu, Phys. Rev. B **78**, 245204 (2008).
[9] J. J. Song *et al.*, Acta. Phys. Sin. **58**, 7947 (2009).
[10] J. E. Dijkstra and W. T. Wenckebach, J. Appl. Phys. **81**, 1259 (1997).
[11] J. J. Song *et al.*, Acta. Phys. Sin. **57**, 7228 (2008).
[12] K. Uchida and M. Saitoh, 9th International Conference on Solid-State and Integrated-Circuit Technology (ICSICT) held at Beijing, China, 978, Oct. 20-23 (2008).
[13] T. Maegawa *et al.*, IEEE Trans. Electron Devices **56**, 553 (2009).
[14] W. H. Seo and J. F. Donegan, Phys. Rev. B **68**, 075318 (2003).
[15] R. N. Sajjad and K. Alam, J. Appl. Phys. **105**, 044307 (2009).
[16] D. Shiri *et al.*, Appl. Phys. Lett. **93**, 073114 (2008).
[17] S. E. Thompson *et al.*, 50th International Electron Devices Meeting (IEDM)
[18] held at San Francisco, USA, 221, Dec. 13-15 (2004).
[19] X. Everett *et al.*, IEEE Trans. Electron Devices **53**, 1840 (2006).
[20] Y. Sun, S. E. Thompson, and T. Nishida, J. Appl. Phys. **101**, 104503 (2007).